



Version 1.X

**Calculation of the Sakuma-Hattori interpolation equation parameters for
calibration of radiation thermometers and blackbody radiation sources**

MANUAL

Gaithersburg, MD • 2013

Content

1. Key Features of Satori111	3
2. Introduction.....	4
3. Theory Basics.....	7
3.1. Multiple-Point Calibration Technique	7
3.2. The Sakuma-Hattori Equation	9
3.3. The Levenberg-Marquardt Method.....	14
3.4. The Particle Swarm Optimization Algorithm	18
4. Working with Satori111	21
4.1. Installing Satori111	21
4.2. Satori111 Database	22
4.3. Entering Initial Data.....	24
4.4. Calculation of Sakuma-Hattori Parameters	26
4.5. Temperature Interpolation with Satori111	28
4.6. Working with Graphs.....	29
5. References.....	31

1. Key Features of Satori111

Satori111 is intended for calculation of parameters in the Sakuma-Hattori interpolation equation and can be used at radiometric temperature calibration of radiation thermometers (pyrometers) and blackbody radiation sources by multiple-point method.

Calculation of Sakuma-Hattori parameters is performed using the Levenberg-Marquardt method then verified by the Particle Swarm Optimization.

Satori111 allows fitting the Sakuma-Hattori equation for up to 20 reference temperatures from 100 to 4000 K with the fitting error not exceeding 1 mK for narrow-band radiation thermometers and 100 mK for wide-band radiation thermometers.

After determination of the Sakuma-Hattori parameters, up to 1000 signals of the radiation thermometer can be converted into temperatures at once.

Satori111 stores the initial data and calculation results in built-in expandable database and represent then in the spreadsheet and customizable and editable graph forms. Data can be copied into the clipboard, exported as text (ASCII), XLS, XML, and HTML table; graphs can be copied into the clipboard, saved as bitmap or Windows metafile, and printed out.

Minimal requirements for hardware and software are:

Processor frequency	1 GHz
RAM	3 GB
Hard disk space	10 MB
Operation system	Windows XP and 7 (32 and 64-bit), Windows 8 in Compatibility Mode

2. Introduction

Radiation thermometry (pyrometry) is the science and technique for non-contact measurements of temperature using thermal radiation emitted by the object. Temperature measured with radiation thermometer can be expressed in various temperature scales such as Kelvin, Celsius, and Fahrenheit.

Thermodynamic (absolute) temperature is one of the principal physical quantities in thermodynamics. It can be derived from fundamental physical laws but its measurement is hard to implement throughout temperature range wide enough for practical applications. The International Temperature Scale of 1990 (ITS-90) [1] is an approximation of the thermodynamic temperature scale designed to facilitate temperature measurements and provide comparability and compatibility of results which can be expressed in Celsius degrees or kelvins. ITS-90 provides equipment calibration standard and includes 17 established calibration fixed points (phase transitions of pure substances), to which temperatures T_{90} from 0.65 K to ≈ 1358 K (from -272.5 °C to ≈ 1085 °C) are assigned. Various thermometer types cover this range of temperatures: helium vapor pressure thermometers, helium gas thermometers, standard platinum resistance thermometers, and monochromatic radiation thermometers. Table 1 shows fixed points and subranges of ITS-90.

ITS-90 implies application of radiation thermometry above freezing point of silver. This means that for temperatures greater than 1234.93 K, measurements of temperature T_{90} can be conducted using the linear pyrometer and the following extrapolation equation:

$$\frac{L_{\lambda}(T_{90})}{L_{\lambda}[T_{90}(X)]} = \frac{\exp(c_2[\lambda T_{90}(X)]^{-1}) - 1}{\exp(c_2[\lambda T_{90}]^{-1}) - 1}, \quad (1)$$

where $T_{90}(X)$ refers to any one of the silver $\{T_{90}(\text{Ag}) = 1234.93 \text{ K}\}$, the gold $\{T_{90}(\text{Au}) = 1337.33 \text{ K}\}$, or the copper $\{T_{90}(\text{Cu}) = 1357.77 \text{ K}\}$ freezing points; $L_{\lambda}(T_{90})$ and $L_{\lambda}[T_{90}(X)]$ are the spectral concentrations of the radiance of a blackbody at the wavelength (in vacuo) λ at T_{90} and at $T_{90}(X)$ respectively; c_2 is the 2nd radiation constant in the Plank law.

Table 1. Defining fixed points and subranges of the ITS-90.

Temperature		Substance	State
T ₉₀ (K)	T ₉₀ (°C)		
3...5	-270.15...-268.15	He	Vapor pressure point
13.8033	-259.3467	e-H ₂	Triple point
≈17	≈-256.15	e-H ₂ (or He)	Vapor pressure point (or gas thermometer point)
≈20.3	≈-252.85	e-H ₂ (or He)	Vapor pressure point (or gas thermometer point)
24.5561	-248.5939	Ne	Triple point
54.3584	-218.7916	O ₂	Triple point
83.8058	-189.3442	Ar	Triple point
234.3156	-38.8344	Hg	Triple point
273.16	0.01	H ₂ O	Triple point
302.9146	29.7646	Ga	Melting point
429.7485	156.5985	In	Freezing point
505.078	231.928	Sn	Freezing point
692.677	419.527	Zn	Freezing point
933.473	660.323	Al	Freezing point
1234.93	961.78	Ag	Freezing point
1337.33	1064.18	Au	Freezing point
1357.77	1084.62	Cu	Freezing point

Methods of radiation thermometry is also used below the silver point [2], for instance, for non-contact measurements of human body temperature, in infrared detection and recognizing of targets, for various industrial applications etc. The fixed-point blackbody radiation sources operating in the temperature range from Hg to Cu freezing temperatures are used for this purpose as well as precision variable-temperature blackbodies [3] working at intermediate temperatures and playing the role of secondary standards.

Extrapolation using Planck's law recommended by ITS-90 for temperature above the Silver point does not satisfy continuously growing modern requirements to reliability and repeatability of high-temperature radiation temperature measurements. This dictates the necessity of developing fixed-points references for temperatures greater than the freezing point of Copper. Currently, the question of introducing additional fixed points (e.g., melting temperatures of some metal – carbon and metal carbide – carbon eutectic alloys) in the future temperature scale is actively discussed [4-6]. Currently,

such unofficial secondary fixed points are already introduced into industrial laboratories to improve temperature calibration above the silver point. Table 2 lists some high-temperature metal – carbon and metal carbide – carbon eutectics together with their *approximate* phase transition temperatures [7].

Table 2. *Approximate* transition temperatures of some metal – carbon and metal carbide – carbon eutectics [7].

Eutectic	Approximate Temperature	
	T ₉₀ (K)	T ₉₀ (°C)
Fe-C	1426	1153
Co-C	1597	1324
Ni-C	1602	1329
Pd-C	1765	1492
Rh-C	1930	1657
Pt-C	2011	1738
Ru-C	2227	1954
Ir-C	2564	2291
Re-C	2747	2474
B ₄ C-C	2659	2386
δ(Mo _x C _{1-x})-C	2856	2583
TiC-C	3034	2761
ZrC-C	3155	2882
HfC-C	3458	3185



The phase transition temperatures of eutectic alloys are not a part of any standard document yet, so they are shown in Table 2 for illustrative purposes only.

3. Theory Basics

3.1. Multiple-Point Calibration Technique

If several reference temperatures near the measured one are available, instead of extrapolation, one can apply interpolation technique which depends less on the linearity of a pyrometer and intrinsic non-linearity of Planck's radiation law. The signal S of a radiation thermometer aimed at a blackbody having temperature T is equal to

$$S(T) = \int_0^{\infty} R(\lambda) L_{\lambda,bb}(\lambda, T) d\lambda, \quad (2)$$

where $L_{\lambda,bb}(\lambda, T)$ is the Planck function at wavelength λ and temperature T ; $R(\lambda)$ is the absolute spectral responsivity of the radiation thermometer.

It is supposed, that $R(\lambda)$ includes such factors as the effective emissivity of the blackbody radiation source, the optical path transmittance, amplifier gain, etc. Since temperatures above the Silver point are determined, according to ITS-90 via the ratio of signals at the unknown temperature and at the reference temperature of the silver, gold, or copper fixed point, it is enough to know only the relative spectral responsivity:

$$r(\lambda) = \frac{R(\lambda)}{\int_0^{\infty} R(\lambda) d\lambda}, \quad (3)$$

which can be measured easier and more reliable than the absolute spectral responsivity.

For the calibration of radiation thermometers near $0.65 \mu\text{m}$, a tungsten strip lamp calibrated against a fixed-point blackbody is often used. For greater wavelengths, due to the large variability of spectral responsivity curves for different types of the infrared radiation thermometers, the calibration against the lamp becomes problematic. In the infrared spectral range, variable-temperature blackbodies are

employed instead of temperature lamps. Accurate temperature measurements via the ratio of the spectral radiances require knowledge of the relative spectral responsivity, since most important components of the uncertainty in the radiometric temperature measurements are conditioned by the uncertainty of the relative spectral responsivity determination. However, measurements of the relative spectral responsivity for the calibration of each radiation thermometer are ineffective and impractical. To resolve this issue, pyrometer readings for several (usually, 3-5) temperatures should be obtained for subsequent interpolation. The main problem here is the choice of the appropriate interpolant, i.e. a function linking pyrometer's signal and measured temperature. Interpolant must contain several adjustable parameters; the number of parameters must be small enough to not embarrass their determination during pyrometer's calibration but provide sufficient flexibility. This approach is often referred to as the multiple point calibration method.

The fixed-point blackbodies, as a rule, provide the best approximation to the perfect blackbody and the least uncertainty in temperature determination. However, other precision blackbody radiation sources (such as heat-pipe and liquid-bath blackbodies) can be used for multiple point calibrations if temperatures of radiators are well-defined or traceable to national temperature standards.

The use of several precision blackbody radiation sources allows not only deriving the calibration equation of the radiation thermometer but also performing the temperature calibration of less-precise laboratory blackbodies.

For the temperature range above the Silver point, the main causes limiting the precision of temperature extrapolation are the non-linearity of the dependence of $S(T)$ which, in turn, depends on the shape of $r(\lambda)$, and non-linearity of the radiation thermometer itself. Introducing high-temperature eutectic fixed points into measurement practice allows employing them as reference points for calibrating radiation thermometers and blackbodies for temperatures up to almost 3000 K using multiple point techniques. Therefore, choosing of an appropriate interpolant for a wide temperature range becomes even more pressing.

A number of empirical equations were developed to this end (see, e.g., [8-10]) and were successfully used for specific wavelength and temperature ranges and for solution of specific measurement tasks.

However, since most empirical interpolants are not based on general physical assumptions, they have limited areas of applicability.

It is known that one can find a polynomial of degree $n > 0$ passed exactly through $n + 1$ arbitrary points on the plane. This means, particularly, that for m pairs of values (S, T) one can always find coefficients for polynomial interpolant of degree $m - 1$ that passes exactly through the measured points. Even if errors in determination of each pair (S, T) are known and the Maximum Likelihood principle (e.g., least square method) is used, there is no guarantee that such an interpolation is physically plausible or gives the best (in some sense) estimate to the actual temperature of the blackbody under measurement. Thence, the interpolant should be physical-based, what means that the adjustable parameters should be directly related to properties of the radiation thermometer.

3.2. The Sakuma-Hattori Equation

Sakuma and Hattori [11] proposed the equation that expresses the signal of the radiation thermometer as a function of blackbody temperature and can be written in form:

$$S(T) = \frac{C}{\exp\left(\frac{c_2}{AT + B}\right) - 1}, \quad (4)$$

where $c_2 = 1.438777013 \cdot 10^{-2} \text{ m} \cdot \text{K}$ is the 2nd radiation constant in the Plank law, A, B , and C are adjustable constants (curve-fitting parameters).

Eq. (4) is known as the *Sakuma-Hattori equation*. Resolving Eq. (4) for temperature gives the *inverse Sakuma-Hattori equation*:

$$T(S) = \frac{c_2}{A \ln\left(\frac{S}{C} + 1\right)} - \frac{B}{A}. \quad (5)$$

Parameters A, B , and C can be found unambiguously if measurements are conducted for at least 3 temperatures. For 3 temperatures, the curve expressing Sakuma-Hattori equation will pass through reference points; if there are more than 3 reference points and the least square technique is applied, the curve will be drawn in such a way that the sum of squared curve-point distances

$$\chi^2 = \sum_{i=1}^n [T_i - T(S_i, A, B, C)]^2 \quad (6)$$

will be minimal. Here and below, n is the number of (S, T) pairs.

The minimal value of χ^2 is reached at the same values of A, B , and C as for

$$\chi = \sqrt{\sum_{i=1}^n [T_i - T(S_i, A, B, C)]^2} \quad (7)$$

The convenient quantitative measure of the interpolation procedure is the root-mean-square (RMS) deviation:

$$\sigma_T = \sqrt{\frac{1}{n} \sum_{i=1}^n [T_i - T(S_i, A, B, C)]^2} \quad (8)$$



**RMS deviation σ_T is not an uncertainty of measurement or calibration.
The value of σ_T characterizes only the curve fitting quality.**

Currently, calibration of low-temperature wide-band pyrometers and variable-temperature blackbodies using multiple points approach with the use of Sakuma-Hattori equation and fixed points of ITS-90 below the Silver point is realized in many national metrological centers and industrial laboratories [12-16] and regulated by national standards (see e.g., [17, 18]). Multiple fixed point calibration method propagates its applicability toward the higher temperatures as high-temperature fixed points are introduced into the practice of radiation thermometry.

Interpolation errors of the Sakuma-Hattori and less common interpolants were investigated in Refs. [19, 20].

Condition $\{\min \chi\}$ is equivalent mathematically to the system of three equations:

$$\begin{cases} \frac{\partial \chi}{\partial A} = 0; & \frac{\partial \chi}{\partial B} = 0; & \frac{\partial \chi}{\partial C} = 0. \end{cases} \quad (9)$$

Although the partial derivatives in the system (9) can be found analytically, the resulting system of non-linear equations can be solved only numerically. Despite the seeming simplicity of Eqs. (4) and (5), numerical solution of system (9) or equivalent minimization problem for expression (6) are not a trivial problem. Two-dimensional plots in Figs. 1 and 2 provide an indication of the complexity of the minimization problem encountered by researchers. These plots were made on the base of two examples included into the database of the Evaluation version of the Satori111 (records “4ITS-90_303-693_11, 6” and “4Eut_2856-3453_0_5, 0_05”). Parameters A, B , and C were determined using the Satori111, then it was supposed that $C = \text{const}$ and χ was plotted as a function of two variables A and B . Such a complicated shape of the objective function χ requires the robust numerical algorithm to avoid the divergence of the computational process and prevent its false convergence to the local minimum in proximity of the initial guess.

The majority of numerical algorithms for finding $\{\min \chi\}$ as well as for the equivalent task of solving the non-linear system (9) require good choice of the initial guess (starting point, or zero approximation). Otherwise, if the objective function is not “good” enough, they may lead to wrong solutions, or even diverge at all as it takes place for the objective function whose A-B slices are depicted in Figs. 1 (for the wide-band infrared radiation thermometer) and Fig. 2 (for the narrow-band radiation thermometer with the mean wavelength of $0.5 \mu\text{m}$).

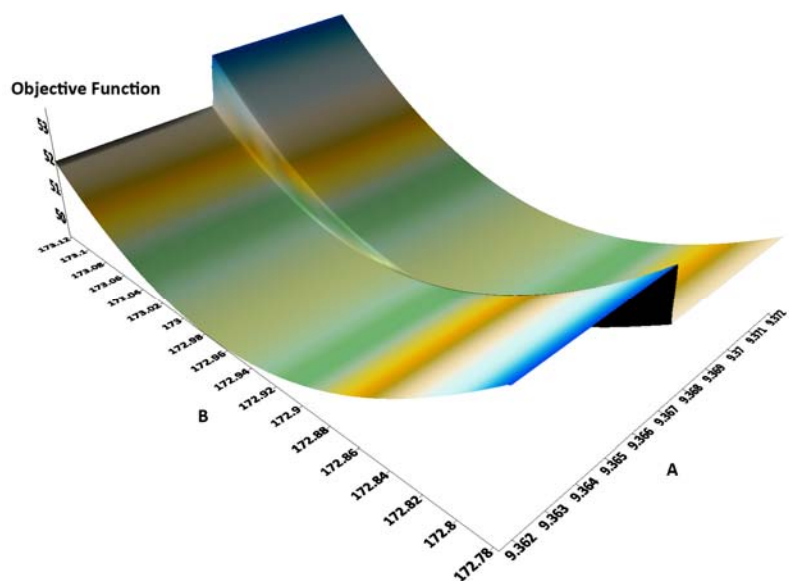


Fig. 1. 3-D surface of $\chi(A, B)$ for the record “4ITS-90_303-693_11, 6”.
The $\min\{\chi\}$ is reached at $A = 9.366866$, $B = 172.94982$, $C = 0.0017269$.

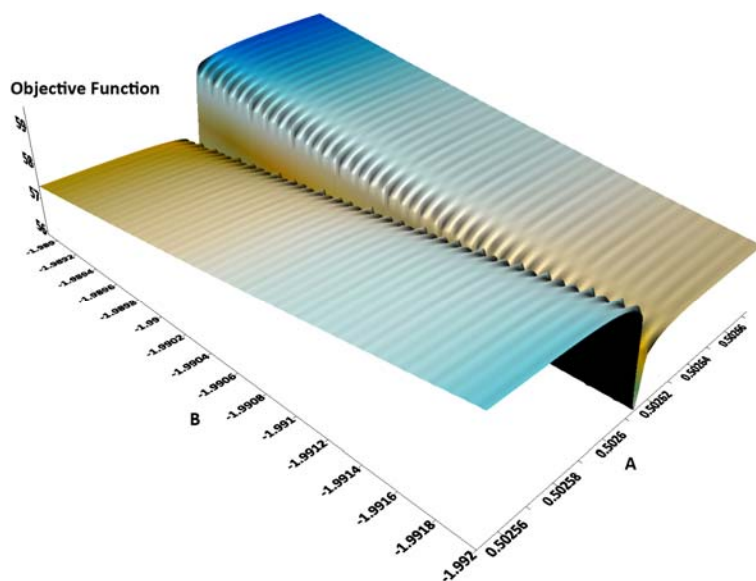


Fig. 2. 3-D surface of $\chi(A, B)$ for the record “4Eut_2856-3453_0_5, 0_05”.
The $\min\{\chi\}$ is reached at $A = 0.50261322$, $B = -1.99085$, $C = 563.2846$.

P. Saunders and R. D. White [21] proposed initial guesses for parameters A , B , and C that are based on the concept of the pyrometer's effective wavelength and the physically plausible assumptions concerning its temperature dependence:

$$A_0 = \lambda_0 \left[1 - 6 \left(\frac{\sigma_\lambda}{\lambda_0} \right)^2 \right], \quad (10)$$

$$B_0 = 0.5 c_2 \left(\frac{\sigma_\lambda}{\lambda_0} \right)^2, \quad (11)$$

$$C_0 = c_1 \int_0^\infty \lambda^{-5} R(\lambda) d\lambda. \quad (12)$$

Here c_1 is the first radiation constant in the Planck law; λ_0 denotes the mean wavelength of the spectral responsivity curve; σ_λ is its variance. Relationships between the variance σ_λ and other, more convenient characteristics of the spectral responsivity curve shape, FWHM (full width at half maximum) are given in Ref. [21] for such shapes as rectangular, triangular, Gaussian, and some others.

Eq. (12) includes $R(\lambda)$ what makes it inconvenient for practical use. Instead, the Satori111 computes C_0 as the mean value:

$$C_0 = \frac{1}{n} \sum_{i=1}^n S_i \left[\exp \left(\frac{c_2}{A_0 T_i + B_0} \right) - 1 \right]. \quad (13)$$

It should be noted that according to Eq. (11) $B_0 \geq 0$, but the resulting B can be negative.

Rigorous mathematical definition of mean value and variation require knowledge of spectral dependence for the spectral responsivity and their integration; however, the easily evaluable FWHM

value can be used instead of variance σ_λ . We will use the term *bandwidth* for a width-like measure of the spectral responsivity curve and *Saunders-White initial guess* for the initial parameters of the Sakuma-Hattori equation computed according to Eqs. (10), (11), and (13).

Determination of Sakuma-Hattori parameters corresponds to the calibration stage of the measurement process. As soon as parameters A, B , and C are found, it is possible to compute unknown temperature T using the measured signal S and the inverse Sakuma-Hattori equation (5). This interpolation procedure corresponds to the measurements stage.

Such an approach is generally used only when unknown temperature point lies between the extreme end points, i.e. for interpolation only. Extrapolation beyond these points is considered as less safe operation. However, as it has been shown in Refs. [22, 23], if the fixed-points have low enough uncertainties and the temperature difference between the highest calibration point and the extrapolated point is small enough, the extrapolation uncertainty in temperatures determined can be comparable with the uncertainty of interpolation within the temperature range under consideration.

Satori111 finds calibration parameters A, B , and C in the Sakuma-Hattori interpolation equation using two independent methods: the Levenberg-Marquardt and the Particle Swarm Optimization.

3.3. The Levenberg-Marquardt Method

The Levenberg-Marquardt (LM) method is a numerical method that provides minimizing a nonlinear function of several variables [24, 25]. Such minimization problems are typical in least squares curve fitting. Due to its robustness, the LM method has become a standard technique for nonlinear least-squares problems and has been used in various numerical mathematics packages for solving non-linear curve-fitting problems.

The LM method can be considered as a hybrid of the steepest descent and the Gauss-Newton algorithms. In the nonlinear least squares minimization for which the LM method provides a solution, the function to be minimized (so-called *objective function*) has the following form:

$$F(x) = \frac{1}{2} \sum_{i=1}^n r_i^2(x), \quad (14)$$

where $x = (x_1, x_2, \dots, x_n)$ is a vector; r_i is a residual; it is assumed that $m \geq n$.

By introducing the residual vector $r(x) = (r_1(x), r_2(x), \dots, r_m(x))$, one can rewrite Eq. (14) in vector form:

$$F(x) = \frac{1}{2} \|r(x)\|^2. \quad (15)$$

The partial derivative can be collected into the Jacobian matrix:

$$J(x) = \left| \frac{\partial r_j}{\partial x_i} \right|, 1 \leq j \leq m, 1 \leq i \leq n. \quad (16)$$

If we consider the case where every r_i function is linear, the Jacobian is constant and one can represent r as a hyperplane in m -dimensional space and F as the quadratic form

$$F(x) = \frac{1}{2} \|Jx + r(0)\|^2.$$

Next, one can obtain $\nabla F(x) = J^T (Jx + r)$ and $\nabla^2 F(x) = J^T J$. The minimum can be found by setting $\nabla F(x) = 0$. As a result, we obtain the solution of the system of normal equations: $x_{\min} = -(J^T J)^{-1} J^T r$.

By analogy, in the non-linear case, we obtain:

$$\nabla F(x) = \sum_{j=1}^m r_j(x) \nabla r_j(x) = J(x)^T r(x), \quad (17)$$

$$\nabla^2 F(x) = J(x)^T J(x) + \sum_{j=1}^m r_j(x) \nabla^2 r_j(x). \quad (18)$$

The important feature of the least square problem is a possibility of deriving the Hessian $\nabla^2 F(x)$ from the Jacobian J if all $\nabla^2 r_j(x)$ are small or all residuals $r_j(x)$ are small (for large residuals, linear approximation can be insufficient; therefore, the performance of the LM algorithm can decrease in such cases). Then the Hessian equals

$$\nabla^2 F(x) = J(x)^T J(x), \quad (19)$$

i.e., the result coincides with that for the linear case.

The conventional gradient descent is the simplest iterative technique for finding a minimum of a function. At $(k+1)^{\text{th}}$ step, solutions are updated by subtraction of the scaled gradient:

$$x^{k+1} = x^k - \xi \cdot \nabla F(x^k).$$

However, the gradient descent method has some convergence problems. To accelerate convergence, it is desirable to set a large step where the gradient is small. From the other side, setting too large step for areas where the gradient is large may lead to skipping the minimum. Besides, the curvature of the error surface (objective function growth rate) can be different in different directions. For example, if there is a long and narrow valley in the error surface, the component of the gradient in the direction that points along the base of the valley is very small while the component along the valley walls is quite large. This results in motion more in the direction of the walls even though we have to move a long distance along the base and a small distance along the walls. This situation can be improved upon by using curvature as well as gradient information, namely second derivatives. One can do this using the Newton method to solve the equation $\nabla F(x) = 0$.

Expanding the gradient of F using a Taylor series around the k^{th} point x^k , one can write:

$$\nabla F(x^{k+1}) = \nabla F(x^k) + (x^{k+1} - x^k)^T \nabla^2 F(x^k) + o(x^{k+1} - x^k). \quad (20)$$

If F is the quadratic form around x^k , one can neglect the higher order terms and solve Eq. (2) for the minimum x by setting the left-hand side of Eq. (20) to zero, one can write the update rule for Newton's method:

$$x^{k+1} = x^k - (\nabla^2 F(x^k))^{-1} \nabla F(x^k). \quad (21)$$

Since Newton's method implicitly uses a quadratic assumption on F (arising from the neglect of higher order terms in a Taylor series expansion of F), there is no necessity to exactly evaluate the Hessian but one can use the approximation (19). The main advantage of this technique is rapid convergence. However, the rate of convergence is sensitive to the starting location (or more precisely, the linearity around the starting location). It can be seen that simple gradient descent and Gauss-Newton iteration are complementary in the advantages they provide. Levenberg proposed an algorithm based on this observation, whose update rule is a blend of the above mentioned algorithms and is given as

$$x^{k+1} = x^k - (H + \xi \cdot I)^{-1} \nabla F(x^k), \quad (22)$$

where H is the Hessian matrix evaluated at x^k , I is the identity matrix. This iterative process works as follows. If, after the current iteration, the error decreases, one can consider the assumption about quadratic growth rate for $F(x)$ fulfilled and one can reduce ξ (e.g., to 10 times) to weaken the influence of the gradient; if the error increases, ξ has to be increased to strengthen the gradient influence. If the error has decreased after the next iteration, the step is accepted and ξ decreases. Iteration ends when the convergence is achieved (that is $|x^{k+1} - x^k|$ becomes less than a given small value δ), or if a maximal number of iterations N_{\max} is reached. In the original Levenberg algorithm [26], for large values of ξ , the Hessian matrix is calculated but not affect the iteration result. D. Marquardt [27] replaced the identity matrix in Eq. (22) with the diagonal of the Hessian matrix. This heuristic substitution leads to larger movement along the directions where the gradient is smaller what allows overcoming the "error valley" problem by scaling each gradient's component according to the curvature of the objective function. The LM iteration process is expressed as

$$x^{k+1} = x^k - [H - \xi \cdot \text{diag}(H)]^{-1} \nabla F(x^k). \quad (23)$$

Satori111 employs a simplified but very fast version of the LM algorithm similar to that described in [28]. Two parameters that determine the stop conditions of the algorithm are Maximal Number of Iterations (N_{\max}) and Tolerance (δ). Their default values are 50 and 10^{-9} , respectively. In most cases, there is no necessity to change them.

Although the LM method is a wide-spread curve-fitting algorithm, it guarantees finding only a local, not a global minimum. Therefore, it is essential to verify the solution obtained by the LM method using another, independent method which is able to find the global minimum, at least, in principle.

3.4. The Particle Swarm Optimization Algorithm

Particle swarm optimization (PSO) is a biologically inspired, population-based, heuristic search and optimization method developed in by and Kennedy and Eberhart [29] and based on social behavior of birds flocking or fish schooling. PSO imitates such a behavior by random movement of “particles” in the multidimensional search space. The movements of the particles are determined by their individual best-known positions as well as the best-known position for a swarm as a whole. Currently, PSO is indispensable algorithm for solving various optimization problems including those with non-convex, non-smooth, and multimodal objective functions. It compares favorably with the best deterministic algorithm because:

- PSO only requires knowledge of lower and upper allowed values for each variable instead of its “good” zero approximations.
- PSO is applicable (at least, in principle) to the global optimization problem.
- PSO is a derivative-free method.

The original PSO algorithm [29] is based on the metaphor that had two cognitive aspects, individual learning and learning from entire group of particles. When a particle determines its behavior, it can use its own experience and the experience of other particles to move itself toward the solution.

If the optimization problem is posed as $\min_{\mathbf{x} \in \Omega} f(\mathbf{x})$, and there is a set of n_{swarm} particles used to search the design space for a function's global minimum, then each particle moves through the space by updating its position with a velocity that accounts for the best position that particle has found and the best position found by all particles. The original updating rule in Ref. [29] is

$$\begin{cases} \mathbf{v}_{j,t+1} = \omega \cdot \mathbf{v}_{j,t} + a_1 u_1 (\mathbf{p}_k - \mathbf{x}_j) + a_2 u_2 (\mathbf{g} - \mathbf{x}_j), \\ \mathbf{x}_{j,t+1} = \mathbf{x}_{j,t} + \mathbf{v}_{j,t+1}, \quad j = 1, 2, \dots, n_{\text{swarm}} \end{cases} \quad (24)$$

where t indicates the iteration number, j indicates the particle number in the swarm, ω is an inertia weighting term, a_1 and a_2 are scalar constants, u_1 and u_2 are random numbers uniformly distributed in $(0,1]$, \mathbf{x} and \mathbf{v} are vectors that indicate the position and velocity of a particle, respectively, \mathbf{p}_k is the best position found by the j^{th} particle, and \mathbf{g} is the best position found by all particles in the swarm.

Clerc and Kennedy [30] modified the PSO algorithm to accelerate its convergence by eliminating the inertia weighting term and using a constriction factor instead. The equation for velocity updating is transformed into

$$\mathbf{v}_{j,t+1} = \chi \cdot (\mathbf{v}_{j,t} + a_1 u_1 (\mathbf{p}_k - \mathbf{x}_j) + a_2 u_2 (\mathbf{g} - \mathbf{x}_j)), \quad (25)$$

where χ is the constriction factor defined as

$$\chi = \frac{2\kappa}{\left| \varphi - 2 - \sqrt{\varphi^2 - 4\varphi} \right|}, \quad (26)$$

$\varphi = a_1 + a_2 > 4$, and $\kappa \in (0,2)$ governs the convergence rate of the iteration process. Clerc and Kennedy [30] recommended the value $\varphi = 4.1$. Satori111 implemented this algorithm for $\kappa = 1$.

More details on various modifications of the PSO method can be found in Ref. [31].

Although PSO does not guarantee locating the global minimum, the probability of its detection is very high at the optimal tuning of the algorithm. To avoid stagnation and convergence to wrong solutions (local minima) Satori111 uses multiple restarts strategy, for which the swarm initialization by random positions and zero velocities is repeated $N_{restarts}$ times. The default value $N_{restarts} = 10$ can be modified by assigning any integer value in the range $[1, 1000]$.

The search domain for Sakuma-Hattori parameters A, B , and C is defined in Satori111 as

$$\begin{cases} A_{\min} = A_0/E, \\ A_{\max} = A_0 \cdot E, \\ B_{\min} = \min(B_0/E, B_0 \cdot E), \\ B_{\max} = \max(B_0/E, B_0 \cdot E), \\ C_{\min} = C_0/E, \\ C_{\max} = C_0 \cdot E, \end{cases} \quad (27)$$

where A_0, B_0 and C_0 are Saunders-White initial guesses computed using Eqs. (10), (11), and (13); $1 \leq E \leq 1000$ is the Search Range parameter; the default value of E is 2.0.

The convenient measure of the fitting quality for both LM and PSO methods is the Mean RMS that is computed as

$$\text{Mean RMS} = \sqrt{\frac{1}{n} \sum_{i=1}^n [T_i - T(S_i, A, B, C)]^2}, \quad (28)$$

where $T(S_i, A, B, C)$ is computed using the inverse Sakuma-Hattori equation.

4. Working with Satori111

4.1. Installing Satori111

Satori111 does not require special installation. Evaluation version of Satori111 is downloadable from www.virial.com. Download *Satori11.zip* and unzip the archive at any convenient place of your hard disk. Do not change mutual arrangement of subfolders in *Satori111* folder. To start working with Evaluation version run *Satori111.exe*. The main window shown in Fig. 3 will appear.

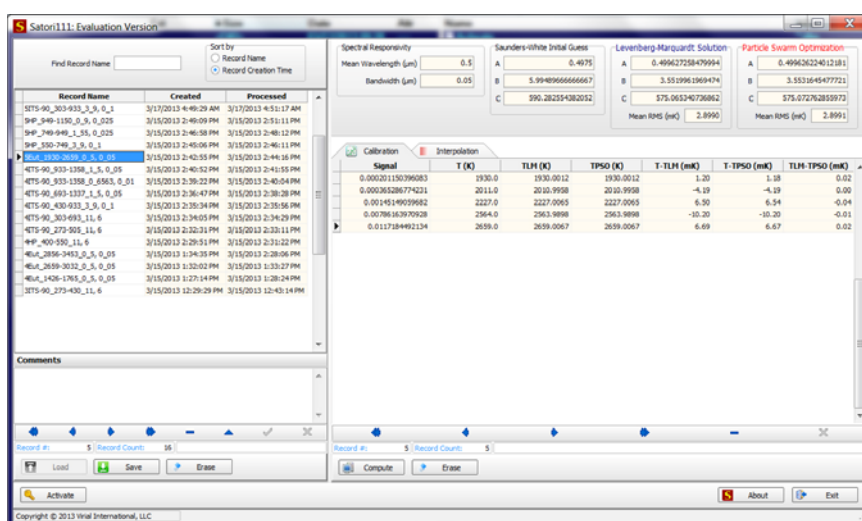


Fig. 3. The main window of Satori111 Evaluation version.

Satori111 will work in the Evaluation mode until its activation. The Evaluation version differs from the full-functioned program at only one point: the Evaluation version does not allow to enter new records into the database intended for permanent storage of initial data and results of calculations. In the Evaluation mode, the database contains only demo examples that, nevertheless, give an idea of Satori111 functionality and principles of operating.

To activate the Evaluation version, you have to purchase the license and obtain the activation key. If you already did this, click the “Activate” button. The Activation window shown in Fig. 4 will appear. Enter your activation key then click “OK”. Fig. 5 shows the main window of Satori111 after activation.

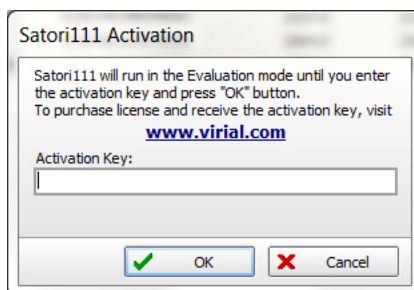


Fig. 4. The Activation window of Satori111.

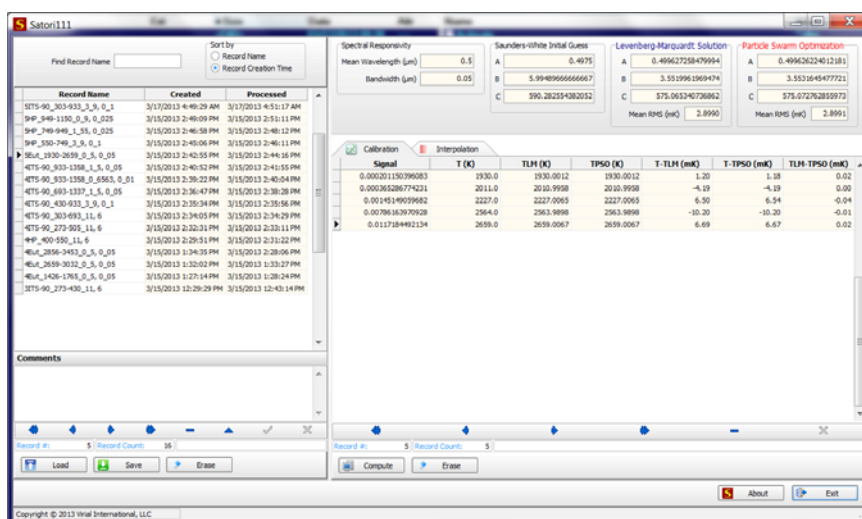


Fig. 5. The main window of Satori111 after activation.

Now, everything is ready to start working with Satori111.

4.2. Satori111 Database

Initial data and results of calculations are permanently stored in the database. Its file *satori111.dbs* is in *DB* folder. Information containing in the database is represented in tabular form. The Satori111 database is presented in two tables or spreadsheets. The first table is placed in the left part of the main window and contains three columns: “Record Name”, “Created” and “Processed”. Only the first column is editable. Above the table, there are the field for incremental search by the record name and the sorting order switch.

The second table is placed in the tabbed page “Calibration” in the right part of the main window and contains the columns described in Table 3.

Table 3. Column description for the table shown in the right part of Fig. 5.

Column caption	Field description
Signal	The signal (in arbitrary units) of the radiation thermometer aimed at the reference blackbody.
T (K)	The temperature (in kelvins) of the reference blackbody.
TLM (K)	The interpolated temperature (in kelvins) computed by the Levenberg-Marquardt (LM) method for the reference blackbody.
TPSO (K)	The interpolated temperature (in kelvins) computed by the Particle Swarm Optimization (PSO) method for the reference blackbody.
T – TLM (mK)	The difference (in millikelvins) between the true temperature of the reference blackbody and its interpolated temperature computed by the LM method.
T – TPSO (mK)	The difference (in millikelvins) between the true temperature of the reference blackbody and its interpolated temperature computed by the PSO method.
TLM – TPSO (mK)	The difference (in millikelvins) between the interpolated temperature of the reference blackbody computed by the LM method and those computed by the PSO method.

Besides, there is the third table placed on the tabbed page “Interpolation” in the right-hand side of the main window (see Fig. 6). This database records contain two fields: the signal of radiation thermometer and the temperature calculated using Sakuma-Hattori interpolation.

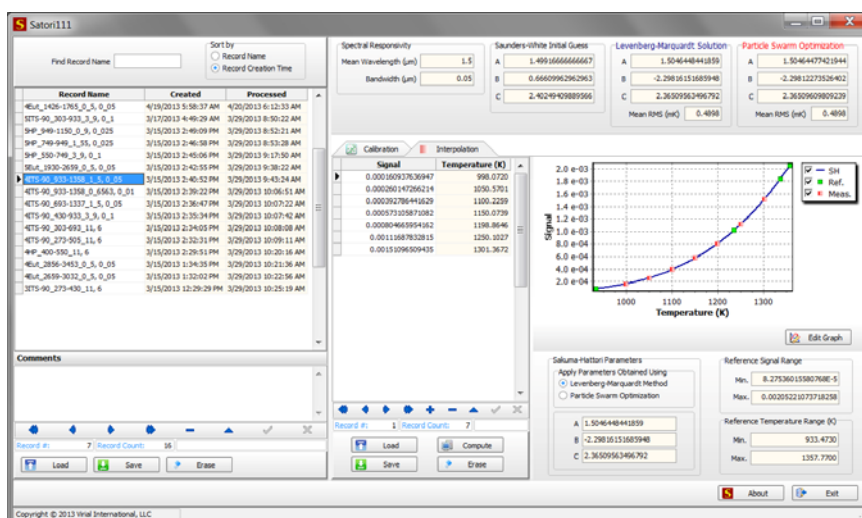


Fig. 6. The tabbed page “Interpolation.”

Below every table there are buttons “Load”, “Save” and “Erase” (or some of them) which allows loading from text file, saving to text file, and erasing a continuous sequence of records at once, respectively.

After clicking “Erase”, the window shown in Fig. 7 will appear. After choosing which records have to be deleted and clicking “OK”, you will be asked for confirmation. Deleted records cannot be restored.

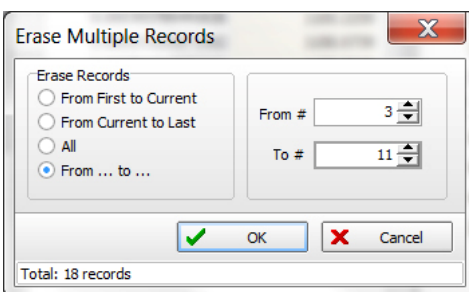


Fig. 7. Erasing multiple records.

Below every table, there is the Database Navigator – the control that provides access to and manipulation with a selected record (see Fig. 8).

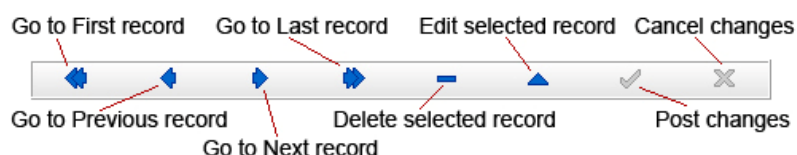


Fig. 8. The Database Navigator.

4.3. Entering Initial Data

To enter a new record into the database, first you have to prepare the text (ASCII) file and place them into the folder *Satori111\Data\Input*. In the same folder, you can find examples of such files that are organized as follows:

```
1.5000 // Mean wavelength in um
0.0500 // Bandwidth in um
4 // Number of reference points
8.27536015580768E-5 933.473
0.00101641821681237 1234.93
0.00184215657521917 1337.33
0.00205221073718258 1357.77
```

The first and the second lines must contain the mean wavelength and the bandwidth, respectively, of the spectral responsivity curve in micrometers. The number of reference points should be specified in the third line. Next lines must contain signals, S_i , (in arbitrary units) and temperatures, T_i , (in kelvins) for the reference points whose number is indicated in the third line. Values of S_i and T_i should be separated by at least one space or <Tab> symbol. Text starting from double slashes is optional; it can be omitted. Such a text file can be prepared in the Windows Notepad or similar text editor.

Once this text file is prepared and saved in the *Satori111\Data\Input* folder, one can enter it into the database by clicking the “Load” button (see Fig. 9). If the text file was prepared and read correctly, Satori111 will request the name for the new record (see. Fig. 10). You can use any sequence of characters for this name; the length should not exceed 100 symbols. Fig. 11 shows the main window after posting the new record.

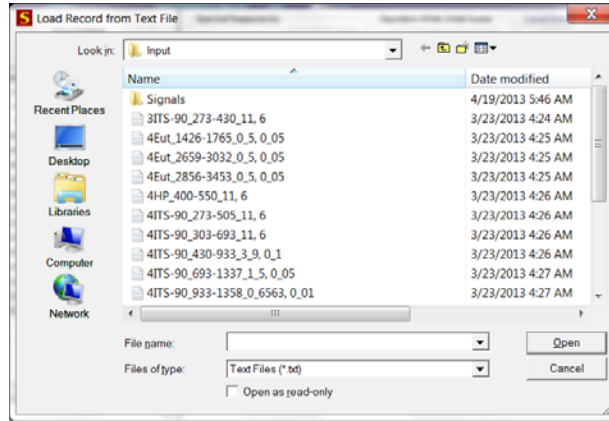


Fig. 9. Loading initial data from text file.

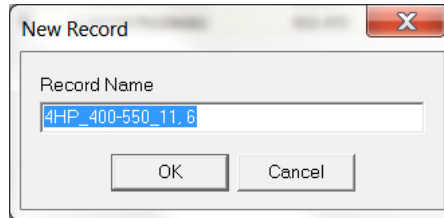


Fig. 10. Request for the name of the new record.

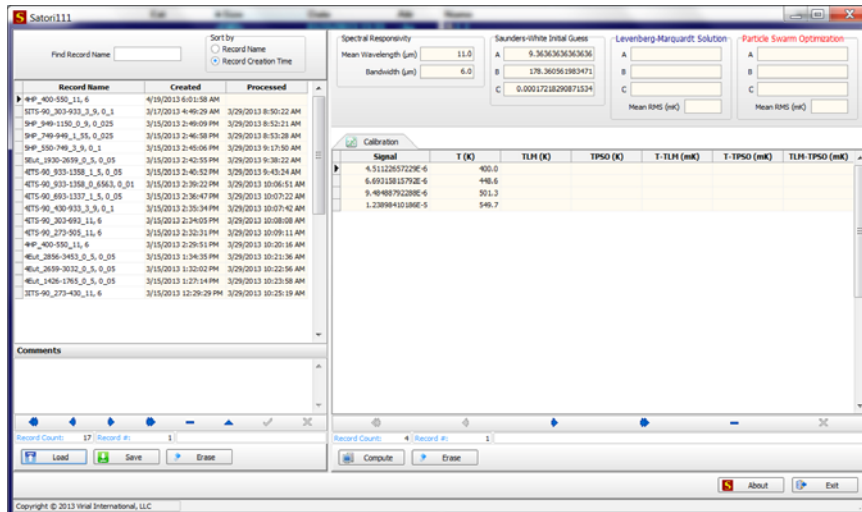


Fig. 11. Main window after posting new record.

Simultaneously with the new record posting, Satori111 performs calculation of the Saunders-White initial guess and displays A_0 , B_0 and C_0 in the appropriate fields at the top of the right-hand side of the main window. Now, one can start calculations of parameters of Sakuma-Hattori equation by clicking the “Compute” button at the bottom of the tabbed page “Calibration”.

4.4. Calculation of Sakuma-Hattori Parameters

Satori111 computes the parameters A , B , and C of the Sakuma-Hattori equation successively, using two independent approaches: the LM and the PSO methods. After clicking the “Compute” button, the window depicted in Fig. 12 will be opened.

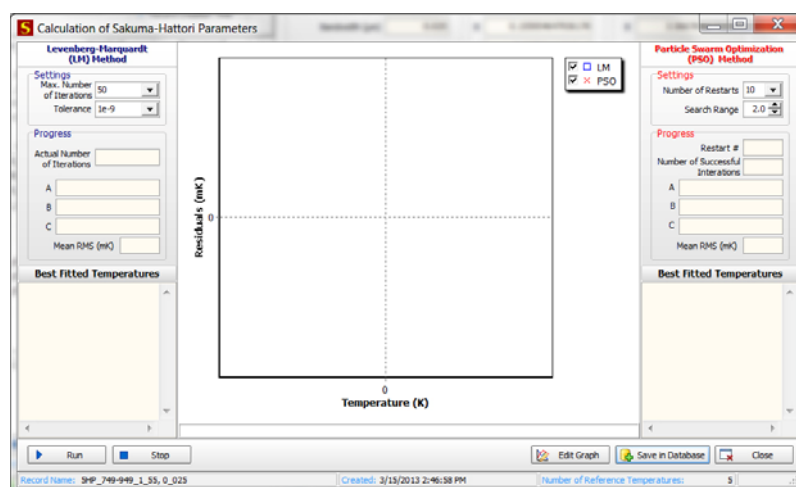


Fig. 12. The “Calculations” window before calculations.

Before starting calculations, one can change settings for both methods: the Maximal Number of Iterations and the Tolerance for the LM method; the Number of Restarts and the Search Range for the PSO method. In most cases, the default values of these settings guarantee the fast convergence of both methods. Click “Run”. Calculations using the LM method are almost instant. If convergence is not reached, the appropriate warning message will be displayed; usually, this indicates an error in the initial data.

Right after displaying the results obtained by the LM method, Satori111 begins fitting using the PSO method. This process can take up to several minutes at the default settings. It is represented in text and graphic forms. The central graph displays the residuals $d_{LM} = T - T_{LM}$ (denoted by the blue squares)

and $d_{PSO} = T - T_{PSO}$ (denoted by the red crosses), where T is the true temperature of the calibration blackbody; T_{LM} and T_{PSO} are its fitted values obtained by the LM and the PSO methods, respectively (see Fig. 13). When the PSO fitting is performed, the fitted temperatures, residuals, and the Mean RMS value are re-displayed at each step accompanied by an improvement of the objective function.

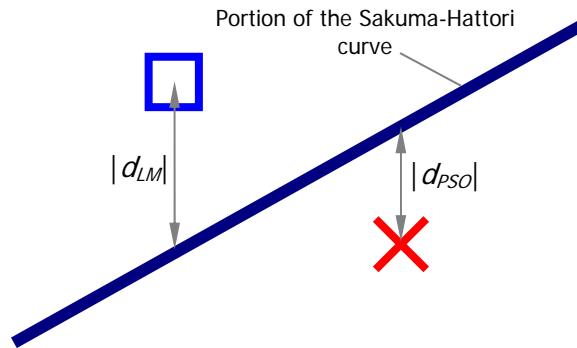


Fig. 13. Absolute values of the fitting residuals.

Fig. 14 shows the “Calculations” window after finishing the fitting. The coincidence of the fitted values within about 1 mK suggests successful determination of the Sakuma-Hattori parameters. One can save results in the database and use the saved parameters later on for any interpolation task based on the same set of reference points. If you don’t want to save results in the database, simply click “Close” and confirm that you decided to ignore the results obtained.

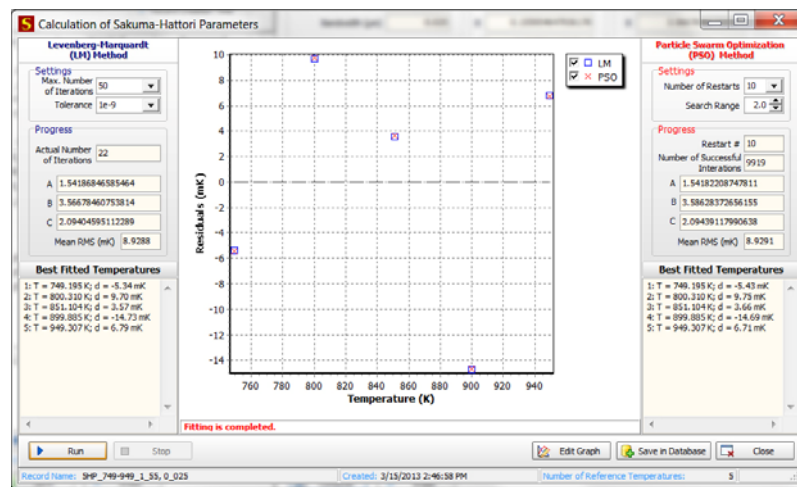


Fig. 14. The “Calculations” window after completion the fitting.

If the absolute value of the difference between results obtained by the LM and the PSO methods is greater than 1-3 mK, it makes sense to check initial data and repeat calculations with the greater values of the Search Range and the Number of Restarts.

User can interrupt the PSO process by clicking the “Stop” button.

4.5. Temperature Interpolation with Satori111

The “Interpolation” tabbed page was shown in Fig. 6. Click “Load” to populate the first column of the table from the text file. Configuration of such a file is very simple (see an example below): the first line must contain the integer number N of signals for which the interpolation has to be performed, then - N lines of signals in the floating point format:

```
11 // Number of signals
1.0657607998996E-5
1.22381158980552E-5
1.41587190884201E-5
1.59467495604791E-5
1.82823504652206E-5
2.04137679389895E-5
2.30209423593449E-5
2.54058415294502E-5
2.83793602690818E-5
3.12380396142741E-5
3.44501551883256E-5
```

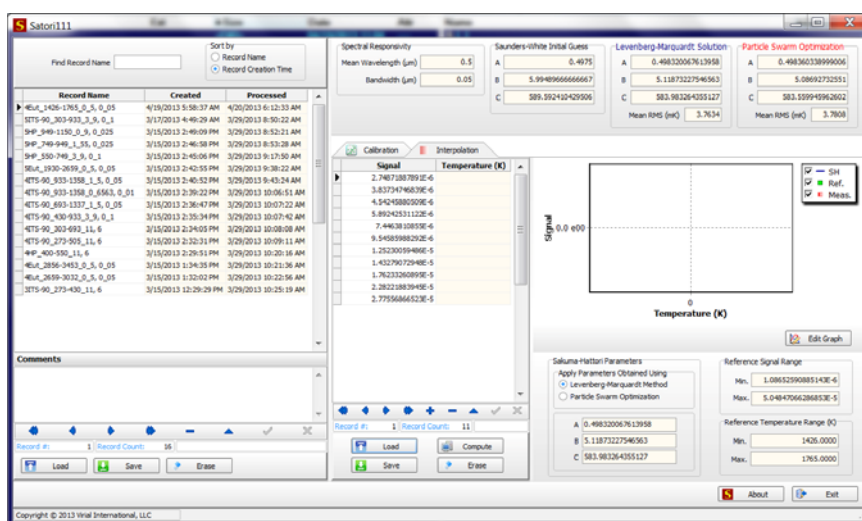


Fig. 15. The tabbed page “Interpolation” for newly entered set of signals.

Multiple other examples can be found in the folder *Satori111\Data\Input\Signals*. Fig. 15 shows the “Interpolation” tabbed page for newly entered set of signals. If you need to perform interpolation only for several signals, one can enter them into the table manually, without composing the text file.

After clicking “Compute”, the table will be populated with the interpolated temperatures, and the graph will be plotted. Data from the table can be saved in the text file by clicking “Save” (Fig. 16).

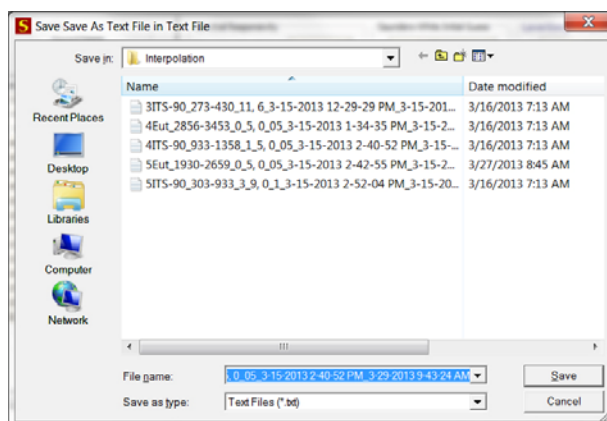


Fig. 16. Saving the results of interpolation in the text file.

Examples of such files can be found in the folder *Satori111\Output\Interpolation*.

4.6. Working with Graphs

All graphs in Satori111 are fully customizable.

User can plot a magnified fragment of the graph: holding left mouse button depressed, drag the cursor right and downwards to zoom and left and upwards to unzoom. To displace curves relative to graph axes, hold the left mouse button depressed and move cursor. To restore graph original position, draw a rectangle of arbitrary size by moving from the bottom right corner to the top left one while left mouse button remains pressed.

Clicking the “Edit Graph” button below a graph calls the Graph Editor, which provides comprehensive access to the properties of the graph via intuitive graphical user interface. The Graph Editor gives the possibility to edit individual curves (series) and all major elements of the graph (points, axes, legend,

title, etc.), copy and save series values in formats of text (ASCII) file, MS Excel spreadsheet, HTML and XML tables, copy to clipboard, save in the file, and print the graphs (see screenshots in Figs. 17-19).



Fig. 17. Graph Editor: manipulating with data series.

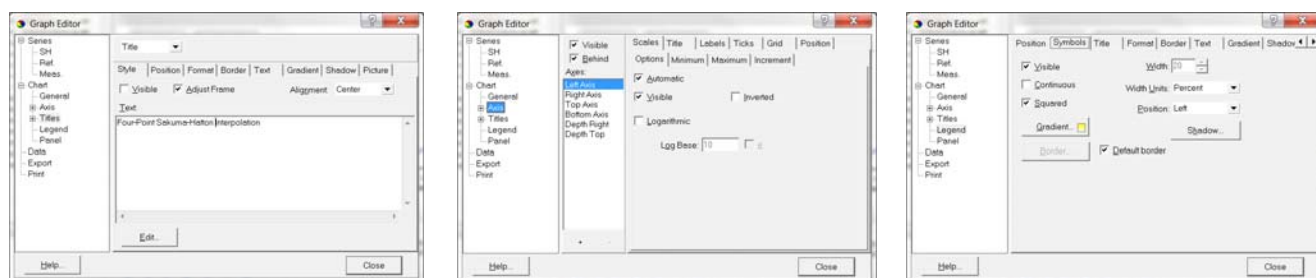


Fig. 18. Graph Editor: editing graph titles, axes, and legend.

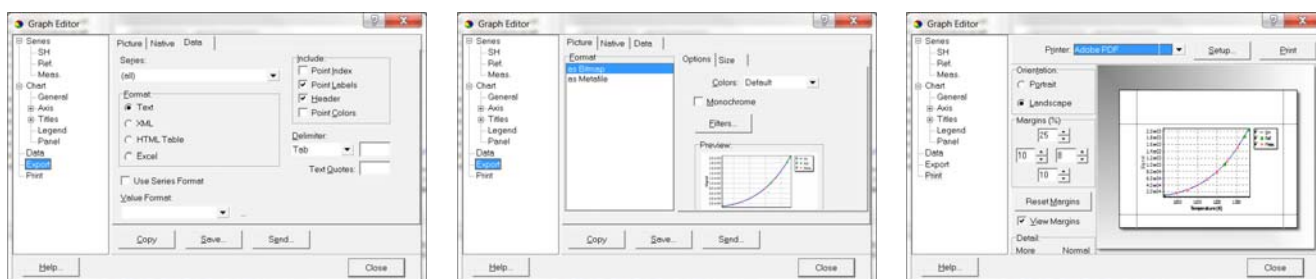


Fig. 19. Graph Editor: exporting and printing ability.

5. References

1. H. Preston-Thomas, “The International Temperature Scale of 1990 (ITS-90),” *Metrologia* **27**, 3-10 (1990).
2. J. Fischer, P. Saunders, M. Sadli, et al., “Uncertainty Budgets for Calibration of Radiation Thermometers below the Silver Point,” CCT-WG5 on Radiation Thermometry, 41 pp. (2008) - <http://www.bipm.org/wg/CCT/CCT-WG5/Allowed/Miscellaneous/Low T Uncertainty Paper Version 1.71.pdf>
3. J. Hartmann, J. Hollandt, B. Khlevnoy, S. Morozova, S. Ogarev, and F. Sakuma, “Blackbody and Other Calibration Sources,” – in *Radiometric Temperature Measurements, v. I. Fundamentals*, Z. M. Zhang, B. K. Tsai, G. Machin, eds., pp. 241-296 (Academic Press 2010).
4. G. Machin, G. Beynon, F. Edler, S. Fourrez, J. Hartmann, D. Lowe, R. Morice, M. Sadli, M. Villamanan, “HIMERT: A Pan-European Project for the Development of Metal-Carbon Eutectics as Temperature Standards,” in *Temperature: Its Measurement and Control in Science and Industry*, Vol. 7, ed. by D. C. Ripple, pp. 285-290, American Institute of Physics (2003).
5. P. Bloembergen, Y. Yamada, N. Yamamoto, and J. Hartmann, “Realizing the High-Temperature Part of a Future ITS with the Aid of Eutectic Metal-Carbon Fixed Points,” in *Temperature: Its Measurement and Control in Science and Industry*, Vol. 7, ed. by D. C. Ripple, pp. 291-296, American Institute of Physics (2003).
6. J. Hartmann, “High-Temperature Measurement Techniques for the Application in Photometry, Radiometry and Thermometry,” *Physics Reports* **469**, 205-269 (2009).
7. E. R. Woolliams, G. Machin, D. H. Lowe, and R. Winkler, “Metal (Carbide)-Carbon Eutectics for Thermometry and Radiometry: A Review of the First Seven Years,” *Metrologia* **43**, R11–R25 (2006).
8. J. W. Hahn and C. Rhee, “Interpolation Equation for the Calibration of Infrared Pyrometers,” *Metrologia* **31**, 27-32 (1994).
9. F. Sakuma, M. Kobayashi, “Interpolation Equations of Scales of Radiation Thermometers,” in *Proceedings of TEMPMEKO '96, 6th International Symposium on Temperature and Thermal Measurements in Industry and Science*, ed. by P. Marcarino, Levrotto & Bella, Torino, pp. 305-310 (1997).

10. F. Liebmann and M. A. C. Carrasco, “Infrared Uncertainty Budget Determination in an Industrial Application,” Simposio de Metrología, Santiago de Querétaro, México (2008) - http://www.cenam.mx/simposio2008/sm_2008/memorias/M1/SM2008-M135-1198.pdf
11. F. Sakuma and S. Hattori, “Establishing a Practical Temperature Standard by Using a Narrow-Band Radiation Thermometer with a Silicon Detector,” in *Temperature: Its Measurement and Control in Science and Industry*, ed. by J. F. Schooley, AIP, New York, Vol. 5, pp. 421-427 (1982).
12. D. Lowe, H. C. McEvoy, and M. Owen, “A Mid-IR Pyrometer Calibrated with High-Temperature Fixed Points for Improved Scale Realization to 2,500°C,” *Int. J. Thermophys.* 28, 2059-2066 (2007).
13. Y. Shimizu and J. Ishii, “Middle Temperature Scale for Infrared Radiation Thermometer Calibrated Against Multiple Fixed Points,” *Int. J. Thermophys.* **29**, 1014–1025 (2008).
14. T. Ricolfi, M. Battuello, F. Girard, G. Machin, H. McEvoy, S. Ugur, and A. Diril, “Radiation Temperature Scales Between the Indium and Silver Points Realized at IMGC, NPL and UME Using a Fixed-point Calibration Technique,” *Meas. Sci. Technol.* **13**, 2090-2093 (2002).
15. P. Saunders, “Calibration and use of low-temperature direct-reading radiation thermometers,” *Meas. Sci. Technol.* **20**, 025104, 8pp. (2009).
16. F. Liebmann, “Infrared Calibration Development at Fluke Corporation Hart Scientific Division,” *Proc. SPIE* **6939** 693906, 11 pp. (2008).
17. E2758 – 10. Standard Guide for Selection and Use of Wideband, Low Temperature Infrared Thermometers. ASTM Standard, ASTM International (2010).
18. MSL Technical Guide 22. Calibration of Low-Temperature Infrared Thermometers. Measurement Standards Laboratory of New Zealand (2009) - <http://msl.irl.cri.nz/sites/all/files/training-manuals/tg22-july-2009v2.pdf>
19. P. Saunders, “Propagation of uncertainty for non-linear calibration equations with an application in radiation thermometry,” *Metrologia* **40**, 93-101 (2003).
20. P. Saunders and D. R. White, “Interpolation errors for radiation thermometry,” *Metrologia* **41**, 41-46 (2004).
21. P. Saunders and D. R. White, “Physical basis of interpolation equations for radiation thermometry,” *Metrologia* **40**, 195-203 (2003).

22. M. Battuello, F. Girard, and M. Florio, “Extrapolation of radiation thermometry scales for determining the transition temperature of metal–carbon points. Experiments with the Co-C,” *Metrologia* **46**, 26-32 (2009).
23. M. Battuello, M. Florio, and F. Girard, “Indirect determination of the thermodynamic temperature of the copper point by a multi-fixed-point technique,” *Metrologia* **47**, 231-238 (2010).
24. W. H. Press, S. A. Teukolsky, W. T. Vetterling, and B. P. Flannery, *Numerical Recipes. The Art of Scientific Computing*, 3rd ed., pp. 801-805 (Cambridge University Press, 2007).
25. Nash, Compact Numerical Methods for Computers. *Linear Algebra and Function Minimization*, pp. 211-215 (Adam Hilger, 1990).
26. K. Levenberg, “A method for the solution of certain problems in least squares,” *Quart. Appl. Math.* **2**, 64–168 (1944).
27. D. Marquardt, “An algorithm for least-squares estimation of nonlinear parameters,” *SIAM J. Appl. Math.* **11**, 431–441 (1963).
28. J. D. Buys and K. von Gadow, “A PASCAL program for fitting nonlinear regression models on a micro-computer,” *EDV in Medizin und Biologie* **18**, 105-107 (1987).
29. J. Kennedy and R. C. Eberhart, “Particle swarm optimization,” *Proc. IEEE Intl. Conf. on Neural Networks*, 1942–1948 (1995).
30. M. Clerc and J. Kennedy, “The particle swarm – explosion, stability, and convergence in a multidimensional complex space,” *IEEE Trans. Evol. Comput.* **6**, 58–73 (2002).
31. M. Clerc, *Particle Swarm Optimization* (ISTE, 2006).